JMEPEG (2018) 27:21–31
https://doi.org/10.1007/s11665-017-2859-4

1059-9495/$19.00

Additive Manufacturing of Catalyst Substrates for Steam–Methane Reforming

Michelle Kramer, Millie McKelvie, and Matthew Watson

(Submitted November 3, 2016; in revised form August 1, 2017; published online August 22, 2017)

Steam–methane reforming is a highly endothermic reaction, which is carried out at temperatures up to 1100 °C and pressures up to 3000 kPa, typically with a Ni-based catalyst distributed over a substrate of discrete alumina pellets or beads. Standard pellet geometries (spheres, hollow cylinders) limit the degree of mass transfer between gaseous reactants and catalyst. Further, heat is supplied to the exterior of the reactor wall, and heat transfer is limited due to the nature of point contacts between the reactor wall and the substrate pellets. This limits the degree to which the process can be intensified, as well as limiting the diameter of the reactor wall. Additive manufacturing now gives us the capability to design structures with tailored heat and mass transfer properties, not only within the packed bed of the reactor, but also at the interface between the reactor wall and the packed bed. In this work, the use of additive manufacturing to produce monolithic-structured catalyst substrate models, made from acrylonitrile–butadiene–styrene, with enhanced conductive heat transfer is described. By integrating the reactor wall into the catalyst substrate structure, the effective thermal conductivity increased by 34% from 0.122 to 0.164 W/(m K).

Keywords monolith, heat transfer, water gas shift, industrial reactor

1. Background and Introduction

1.1 Pellets and Traditional Steam–Methane Reforming Catalysts

Steam–methane reforming is a highly endothermic process that has been industrially relevant for over 80 years and is currently responsible for approximately half the world's hydrogen production (Ref 2). There are three main types of reformers, which are differentiated by their heating mechanism. These include top-fired reformers, bottom-fired reformers, and terrace-walled (side-fired) reformers (Ref 27). The tubes inside of these reformers are typically between 10 and 12 m long, have an outer diameter between 70 and 160 mm, and a wall thickness of 10-20 mm (Ref 29). The tubes are almost exclusively constructed of nickel–chromium alloys due to their favorable high-temperature properties and their contribution to the steam reforming catalytic process, as most industrial catalysts use a nickel-based catalyst (Ref 30). The tubes are generally filled with a catalyst that is supported on pellets of a high surface area substrate such as gamma-alumina (Ref 9). Unfortunately, due to their non-integrated, discrete nature and the properties of ceramic substrates, there are heat and mass transfer limitations that mean the efficiency of this process can only be approximately 65-75% (Ref 3). The heat transfer limitations arise from the tube being heated to 1000-1100 °C, but there only being "point" contacts between the tube wall and the catalyst pellets and the same between catalyst pellets inside of the reformer tube. This leads to a radial temperature gradient as well as "hot-spot" formation along the reformer tubes. These hot spots are detrimental to the microstructure of the tubes, as the tube life is exponentially influenced by the temperatures that the tubes experience, e.g., tubes held at 1050 °C will undergo creep and other injurious behaviors much faster than tubes held at 900 °C. High-alloy metals are able to withstand roughly half of the stress over a period of time when the temperature is varied from 900 to 1000 °C (Ref 16). This is important because replacing tubes inside a reformer is a very costly procedure (Ref 25).

The catalyst and its support are a major point of possible improvement in the SMR process. Process intensification can be achieved by modification of catalyst design from two approaches—modification of the structural configuration or modification of the functional configuration. One of the major issues with process intensification through structural modification is that it spans the macro- and microscale, which until very recently has been limited by existing technologies for ceramic substrate production and subsequent catalyst coating and activation (Ref 3).

Another concern of the catalyst substrates is related to the distribution of catalyst on the support which has mass-transfer-limiting issues. The reaction rate within a reformer tube is strongly influenced by the limitations of gas-phase diffusion within the micropores of the support. Lower catalyst effectiveness is linked to large catalyst pellet sizes, but smaller catalyst pellet sizes are strongly unfavorable due to their effect on the pressure drop (Ref 28). Other geometries have been proposed to eliminate the issues seen with a packed bed of catalyst pellets. One alternative that has been thoroughly researched is a monolithic structure, which has been used to great effect in many environmental applications and has some significant advantages over the use of catalyst pellets. The advantages and disadvantages of this geometry are further discussed in this paper, but the focus is on the clearance present between a monolithic catalyst structure and the tube containing it. Since

Michelle Kramer and **Matthew Watson,** Chemical and Process Engineering, University of Canterbury, Christchurch, New Zealand; and **Millie McKelvie,** L.E.K. Consulting, Sydney, NSW, Australia. Contact e-mail: matthew.watson@canterbury.ac.nz.

heat transfer and mass transfer at high temperature are so important to this process, it makes sense to try and understand the obstruction to heat transfer that a gap between the monolith and the tube wall represents. This paper addresses our current understanding of the presence of the gap to efficient heat transfer, areas for further development of this understanding, and spheres for further research including the use of additive manufacturing to reduce gap effects.

The motivation behind this research is to increase the efficiency and reliability of catalyzed reactions, especially highly endothermic, heterogeneous, mass-diffusion-limited catalyzed reactions. These types of reactions use multi-material systems and therefore have boundary layer limitations and 3D printing may resolve these limitations. The rest of this paper will expound upon this and other related ideas.

Traditionally, in steam–methane reforming, packed beds of catalyst pellets have been used. Over the years, the pellets have been changed in shape to help optimize the pressure drop and catalytic activity of the process. The pressure drop increases as the pellet size decreases, but the catalytic activity increases with surface area (generally resulting from a greater number of smaller pellets).

1.2 Monoliths

Monoliths generally have many advantages over packed beds including: higher mechanical strength, more even flow distribution, improved heat transfer, lower pressure drop, and improved mass transfer performance (Ref 39). Using monolithic catalysts, even though they are typically made from materials with low thermal conductivity, changes the dominant mode of radial heat transfer inside of the reactor to conduction which demonstrates significant improvement in both radial and axial heat transport not present in packed bed reactors due to lack of connectivity (Ref 12).

Despite the numerous advantages of monoliths, there are a few disadvantages, including higher cost of manufacture, misdistribution or lower loading of the active phase of the catalyst, new catalyst fabrication procedures would have to be implemented, and the monoliths cannot currently be manufactured in very long lengths (since the tubes are typically 10-12 m in length) so multiple monoliths would need to be stacked on one another (Ref 39). In addition to the disadvantages of monolithic catalysts outlined by Zamaniyan et al. (Ref 12), typical ceramic parallel channel monoliths are essentially adiabatic, which makes temperature control of the process fluid inherently difficult.

Monolithic-structured supports can lead to an increase in space velocity (allowing the required size of the reactor to be reduced, which has applications in fuel cells). One study by Farrauto et al. showed up to 10 times the space velocity of an equivalently sized packed bed reactor, although Farrauto points out that combining this reaction with another reaction that is highly endothermic in a heat exchanger-like structure would be necessary to provide the required heat flux. This is because heat transfer resistance is a controlling factor in traditional packed bed reformers. The pressure drop, in this same study, was shown to decrease by 80-90% in monoliths with high open frontal areas, potentially saving on energy utilization and energy costs associated with process gas compression. Monoliths that are wash-coated with a highly active metal catalyst (specifically using precious metals such as Rh, Ru, and Pt) have even shown greater resistance to the chemical and mechanical degradation that typically occurs during reactor start-up or shutdown (Ref 9).

Using a monolithic catalyst form also typically introduces a gap between the monolith and the reactor wall. There are many approaches being researched in order to minimize the effect of this gap on heat transfer between the monolith and the reactor wall (Ref 12). Zamaniyan et al. have proposed the use of a tube-fitted bulk monolithic catalysts (TFBMCs), which are monoliths that are spaced to generate fluid mixing between each piece and are constructed completely of the active phase of the catalyst in order to promote active surface area. These TBFMCs were wrapped in a metal sheath to promote heat transfer and assist with issues commonly encountered with monoliths including crushing with temperature fluctuation, easier loading and removal, and a way to overcome the theoretical gap present between the bulk monolithic catalyst and the wall of the reactor tube (Ref 39). In an article by Tronconi et al. (Ref 35) experiments were conducted with different monoliths, each with different thermal conductivities. A copper honeycomb monolith showed no radial temperature profile, just a varying temperature profile along the length of the monolith as the reaction neared completion. They also experimented with ways of reducing the gap effect between the monolith and the wall of the reactor. When they used aluminum fins to allow for conduction between the monolith and the wall, film heat transfer coefficients between 400 and 500 W/(m^2K) were measured. Boger and Heibel performed a study on the effect of the gap between conductive monoliths inside a tube, with the tube immersed in a jacket of cooling water to keep the section between the inlet and outlet of the cooling jacket isothermal (Ref 4). When the group investigated the same monolith with no special treatment to increase contact between the monolith and the wall, the film heat transfer coefficient was about half of what was able to be achieved with enhanced monolith to wall contact (Ref 35).

In terms of the honeycomb structure, no radial convection takes place within the channels, which concurs with an earlier study (Ref 35). However, high conduction rates may occur throughout the solid structure, depending on the thermal conductivity of the material and the void fraction, again in agreement with the earlier article by Tronconi et al. The size of the gap between the monolith and the tube influences the heat transfer resistance significantly. It was determined that the greater the clearance between the catalyst and the internal tube wall, the greater the heat transfer resistance (Ref 4) and the greater the risk that a significant portion of the process gas will bypass the monolith altogether. Boger and Heibel make a more detailed study of the gap between monolith and the wall without any sort of enhancement of the heat transfer to try and better understand the effect of the gap. Since it has been demonstrated that the size of the clearance at the monolith–tube interface is of significant importance in heat transfer, forming a monolithic structural support that has dimensions as close as possible to the inner diameter of the reactor tube would be a prudent path forward to mitigate heat transfer limitations. However, there is a trade-off between the improved performance from small clearances and ease of loading. It has been shown that for clearances of 50-100 μm, force was required to insert the monoliths into a tube (Ref 4). This poses a significant challenge considering reformer tube length is typically between 10 and 12 m, and catalyst crushing is a significant concern within industry (Ref 27).

1.3 Fabrication via Additive Manufacturing

The most popular method of additive manufacturing, or 3D printing, in metal is currently a process called selective laser melting. This process involves using a laser to selectively and partially melt metal powder into a specific shape for a desired layer (of specific thickness that depends on the printer resolution). More powder is added to the bed, and the sintering/melting process is repeated. This procedure is repeated until the desired part is completed, then the extraneous powder is purged from the bed (usually via a vacuum process), and the remaining part is removed (Ref 6).

Electron beam melting (or EBM) is gaining ground for its unique ability to process alloys that are traditionally difficult to manufacture, like Grade 5 Titanium (Ti-6Al-4V), which is primarily used in the aerospace industry (Ref 38). EBM is also useful for building complicated structures of variable porosity. The electron beam is controlled by changes in an electromagnetic field rather than a change in position of mirrors as in selective laser melting. This allows for a greater degree of control, but can only be used with electrically conductive materials (Ref 13).

For printing in ceramic, there are many technologies that have been invented and are currently the subject of much research. There are not currently any particular front runners for wide applicability since most technologies require post-processing of some sort, generally sintering the green body produced by the additive manufacturing device. Direct ink writing, or robocasting, was one of the first technologies that produced a fully dense ceramic part. Robocasting uses a ceramic "ink" that is extruded from a nozzle in a manner similar to fused deposition modeling (FDM) in plastic. The "ink" development is the most crucial aspect of this type of printing, due to the necessary rheological properties for printing and the later polymer removal during sintering (Ref 19). 3D printing using a liquid pre-ceramic resin is a fairly new technology introduced in early 2016. This method makes use of photosensitive polymers and existing stereolithography machines to cure the resin in a layer-wise fashion, making parts of mostly uniform shrinkage and no porosity according to an article published in Science (Ref 7).

Selective laser melting can also be used for ceramics, the advantage of using SLM being that there is no post-processing sintering step, just removal of extraneous powder (Ref 18). Lithography-based ceramic manufacturing is another type of process that does not require a secondary or post-processing step due to the nature of the process. A photosensitive suspension consisting of a ceramic, photoinitiator, monomer, and various additives is exposed to light through a complex arrangement of mirrors and light-emitting diodes (LEDs), which results in a fully dense part. Schwentenwein and Homa achieved an alumina density of over 99.3% of theoretical using this method (Ref 32).

A number of these technologies can actually be used in multi-material printing, theoretically allowing for a co-printed substrate with catalyst inside a pressure-containing chamber. Ceramics and metals could be printed using the same machine, the same method, and be fully functional parts for an end user (Ref 34). 3DP is a process invented at the Massachusetts Institute of Technology's CSAIL (Computer Science and Artificial Intelligence Laboratory) in 1993. The process utilizes a liquid binder that is applied to a powder layer in a specific pattern according to that "slice" of the part. Next, more powder is applied and more binder applied in the shape of the next "slice". The surrounding powder acts as a support and can be removed after the part has finished printing, generally by vacuuming or similar dust removal process (Ref 14). Care needs to be exercised with this method due to the process utilizing large amounts of powder. Powder for this process can be metal, ceramic, plastic, composite, or mixtures of these as long as the binder(s) used are compatible with the powders used and are able to hold the shape of the green body prior to post-processing. Post-processing consists of either chemical treatment or sintering. Plastics are frequently post-processed via chemical treatment, while metals and ceramics are mostly post-processed via sintering due to inherent material properties (Ref 31).

3D printing of monoliths is not a totally new idea within chemical engineering unit operations. This process has been utilized to produce columns for chromatography with a range of highly homogeneous internal structures (Ref 10). As a proof of concept, Fee et al. demonstrated that the column, packing, distributors, and fittings can all be printed in a single piece, reducing operational complexity. It was also found that in a honeycomb structure, flow distribution was not completely uniform and some parts of the column were not utilized, but introducing a fractal distributor corrected for the misdistribution. Bead-like structures that were 3D-printed, but uniformly arranged, were also studied, and it was found that radial mixing was greatly improved (Ref 26). Octahedral beads were printed in these columns with different degrees of overlap (varying the porosity while keeping other variable constants, i.e., particle arrangement and tortuosity). Porosity has an opposite effect to what is expected in packed bed columns, controlling for other variables. This led to an important discovery with respect to chromatography in that porosity was not really the variable to control, but instead the uniformity of the flow channels (Ref 26).

Since additive manufacturing is a relatively new technology, there is much research to be performed involving the understanding of the material properties relative to traditionally manufactured components—especially with regard to catalyst and catalyst support manufacture. While some research has been performed on metals and ceramics relating to the compressive strength, yield strength, and other similar properties, there has been little research carried out using additive manufacturing for pressure vessels. This would be critical if an integrated structure were to be developed, resulting in co-printing of the catalyst structure and the tube wall. This has possible applications in many industries including aerospace, chemical and petrochemical, pharmaceutical, robotics, and maritime, to name a few. Prototypes for pressure relief in plastic have been printed and been liquid pressure tested to fracture at 460 and 580 psi or approximately 3.2 and 4.0 MPa, but after further revision of part design, the part did not burst until 1150 psi or 7.9 MPa. These prototypes were produced using stereolithography (Ref 1). This technology will need to be further explored for the materials and methods being used in these experiments to allow more research to be conducted on 3D printing catalysts that are integrated with tube walls to allow for improved heat conduction and mass transfer. These investigations should also be explored for multi-material printing for applications at high temperatures and pressures. This could greatly affect the chemical catalysis industry as many of these reactions are performed at high temperatures and

pressures, but require a combination of materials in order to facilitate the catalytic reaction.

Of the three main material classes (plastics, metals, and ceramics), plastics are the lowest cost material choice when producing a conceptual design or prototype. The most widely adopted method of 3D printing in plastic is a process called fused deposition modeling, or FDM. This method was used to produce the prototype monoliths tested in this study. The printer used was a Stratasys Dimension Elite. Acrylonitrile–butadiene–styrene, or as it is commonly known, ABS, is typically used over a temperature range between −30 and 90 °C (Ref 15). Therefore, the experiments that were carried out using ABS thermoplastic are only applicable to a much lower temperature range than what is used in steam–methane reforming. However, ABS is used here as a proof of concept before proceeding to further studies using more industrially relevant materials such as alumina-based ceramics and nickel-chrome super alloys.

2. Methods

2.1 Material and Shape Selection and Constraints

Through SolidWorks CAD software (Dassault Systèmes SolidWorks Corp, USA), four structured catalyst substrates were designed and then converted to a compatible format for printing at the University of Canterbury's Additive Manufacturing facilities (Christchurch, New Zealand). The design of the catalyst was subject to the following constraints:

- The print material must have a thermal conductivity at least an order of magnitude greater than that of stagnant air. The thermal conductivity of air is approximately 0.024 W/(m K) at the conditions of interest. The material chosen was acrylonitrile–butadiene–styrene (ABS P430), which has a conductivity ranging from 0.18 to 0.33 W/(m K) (Ref 11).
- The length of the integrated catalyst and tube (cylinder) was required to be four times the diameter. This ensured that the effect of axial heat flow at the mid-plane was negligible as the bed is of sufficient length (Ref 17).
- To ensure that the size of the component was reasonable, the diameter of the cylinder was to be as small as possible. However, the printed structure must be free of AM faults and symmetric about the mid-plane. Hence, no detail within the design can be less than 1 mm.
- The "gap" at the monolith–tube interface is to be designed as small as possible. Nevertheless, it must be uniform in thickness around the circumference and along the length of the cylinder.
- The cylinder must be completely sealed for experimental purposes.
- The design must accommodate a thermocouple through the center axis of the cylinder and should reach halfway through the length of the monolith. The thermocouple must maintain good contact with the plastic.

The initial design concepts for the monolith structures are shown in Fig. 1. The cross sections show the internal straight channel monolith structures and model the gap between the reformer tube and catalyst support.

The first concept with the circular internal pattern was proposed by Zamaniyan et al. (Ref 39) in their investigation of a tube-fitted bulk monolithic catalyst (TFBMC). This design is potentially ideal because it displays no non-uniformity across its cross section. The second concept, a square-hole monolith structure, was suggested as a similar design was previously investigated by Boger et al. (Ref 4) and Groppi et al. (Ref 12). The third structure is an unconventional, biomimetic monolith design based on the cross section of many types of fruit (e.g., an orange), whose structure allows for efficient nutrient transfer throughout the fruit. This proposal contrasted to the square- and circular-hole straight channel monoliths as it would provide direct paths for heat conduction. The third proposed structure will be modified later to keep the direct paths for heat conduction but also allow for flow mixing, and in fact only the square-holed structure was experimentally characterized in this work.

2.2 CAD and Printing

Each structure was drafted in SolidWorks and designed to have the same void fraction. Several small examples were printed using a Stratasys Dimension Elite printer using material ABS*plus* P430, which is a proprietary ABS material. These were printed in cooperation with the Mechanical Engineering department in the 3D Printing and Additive Manufacturing suite located at the University of Canterbury. These samples showed that the minimum resolution chosen (1 mm) yielded issues with consistent performance in the internal structure, and so a larger size was chosen for the distance between channels. The printer used the following settings for printing and treatments were applied to all four ABS cylinders:

The new sample had a structure similar to that of the paper by Boger and Heibel, using parallel, square channels. The size of the squares was 1.9 mm, and the distance between each was chosen as 1.8 mm. The squares were arranged in such a way

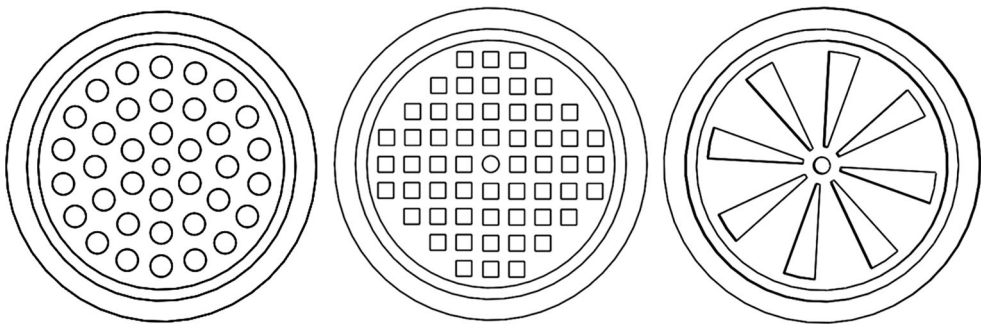

Fig. 1 Circular, square, and biomimetic internal structure proposals

that the structure is very clearly defined, symmetric about the mid-plane, and displayed no visible defects as shown in Fig. 2.

As the above structure is compatible with the printer bed dimensions subject to the earlier listed constraints, this pattern was selected for experimentation (Table 1).

In addition to the straight channel monolith designs, a solid ABS cylinder which represented a perfect heat conduction scenario was proposed to be printed. This prototype embodied negligible heat transfer resistance over the gap or within the channels of the monolith. Essentially the cylinder was to act as a control for the experiment, so that the thermal conductivity of the given ABS plastic could be measured. To complement this cylinder, an identical solid model with the addition of a gap clearance between the monolith and the inner tube wall was also designed and manufactured. Tables 2 and 3 outline the key dimensions of these samples.

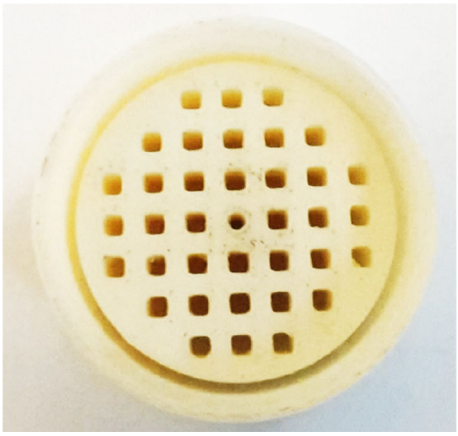

Fig. 2 ABS square-hole monolith with 35 mm diameter

Table 1 Printer settings for Stratasys dimension elite printer

Printer setting or treatment	Possible values and *value used*
Model interior	Spare-low density, *sparse-high density*, solid
Layer height	*0.178 mm*, 0.254 mm
Support fill	Sparse, basic, *SMART*, surround
Part treatment for support removal	Soak in 5% caustic at 70 °C
Material	ABS*plus*—ivory

The thermocouple well terminates halfway through the length of the monolith, located at axial and radial center of the cylinder.

The cross sections of the substrates that were selected for printing are given in Fig. 3.

As shown in the work of Uddin et al. (Ref 36), the settings used for printing an ABS FDM part have a large impact on the mechanical properties of that part as compared to a part manufactured through injection molding. They also concluded that the mechanical properties are strongly anisotropic. The anisotropy of thermal properties was not assessed in this study as all monoliths were printed in the same vertical orientation resulting in circular patters being layered on top of each other. We would therefore not expect any significant anisotropy of the average thermal properties in the radial direction (Fig. 4).

2.3 Heat Transfer Characterization

Sheng et al. (Ref 33) measured the thermal conductivity of a series of MFEC monoliths by inserting the catalyst support into a copper tube and submerging the arrangement in a water bath.

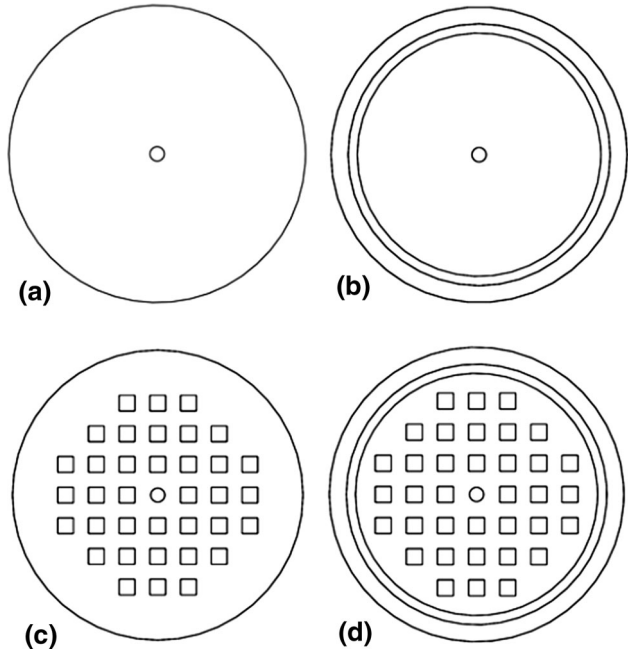

Fig. 3 Cross sections of final concepts for AM: (a) solid; (b) solid with gap; (c) squares; (d) squares with gap

Table 2 Key dimensions of solid cylinders

Material		ABS plastic	
Description	**Unit**	**Solid**	**Solid with gap**
Outer diameter of cylinder	mm	35	35
Tube width	mm	2	2
Inner diameter tube	mm	31	31
Gap width	mm	0	1.2
Outer diameter monolith	mm	31	28.6
Length	mm	140	140
Length of thermocouple well from top face	mm	70	70
Thermocouple well diameter	mm	1.7	1.7

Thermocouples were used to measure the temperature change with time over the cross section of the support in order to determine the effective thermal conductivity. The tube was filled with stagnant nitrogen gas at ambient pressure. A similar method was proposed for measuring the thermal conductivity of the ABS 3D-printed monoliths.

As the cylinders were built via additive manufacturing, they had a slightly porous structure. Hence, for the experimental method to be appropriate it was essential that each sample was completely sealed. This was in order to ensure that stagnant air at atmospheric pressure was trapped inside the cylinder and that water could not enter the internal structure. The thermal conductivity of water is 0.584 W/(m K) at the conditions of interest which is greater than the 0.18-0.33 W/(m K) of the ABS plastic (Ref 8, 24). Any water within the structure would significantly alter the results.

To prevent the entry of water, each cylinder was wrapped with a 0.1-mm film of polypropylene plastic. Due to the thinness of the wrapping and its similar thermal conductivity properties to ABS plastic, the overall thermal conductance of the test piece was not affected (see "Appendix" for a detailed analysis). The top end of the cylinder (where the recessed portion was located) was sealed with a transparent circular polycarbonate disk through the use of Sikasil Silicone Sealant. A thermocouple was then fully inserted into the thermocouple well. The thermocouple tip was coated with Dow Corning 340 silicone heat sink compound in order to ensure that the tip of the thermocouple had sufficient contact with the solid cylinder. The area where the thermocouple entered the structure was then covered with the same silicon sealant to guarantee that water did not enter the structure.

Once the structure was water tight, the thermocouple was linked to an EL-USB-TC-LCD thermocouple data logger. The data logger had a USB function which plugged into the complementing software program installed on a laptop. The data logger was preset to begin recording when the button was pressed and to provide a display of the temperature reading every second. The logger was programmed to record a temperature reading every 10 s. To stop recording, the data logger was required to be plugged into the Laptop USB socket and "stop recording" selected in the program options.

Each cylinder (at room temperature) was then horizontally immersed in a water and ice bath at 0 °C. Clamps at one end of the cylinder were used to ensure that the model remained submerged, while the temperature of the bath was monitored via a CHY 805 RTD Thermometer. When the thermocouple indicated that the mid-plane temperature of the cylinder had reached zero, the temperature of the cylinder was considered uniform about its volume. The sample was then quickly transferred to a prepared 30 °C stirred water bath. At $t = 0$, the data logger recording was initiated. The cylinder was then left to heat, until a steady temperature of 30 °C was achieved. Recording was then stopped and the data downloaded. The process was repeated, taking the model from 30 to 0 °C. Three trials for each water bath type were carried out. A simplified diagram of the heated water bath is provided in Fig. 4.

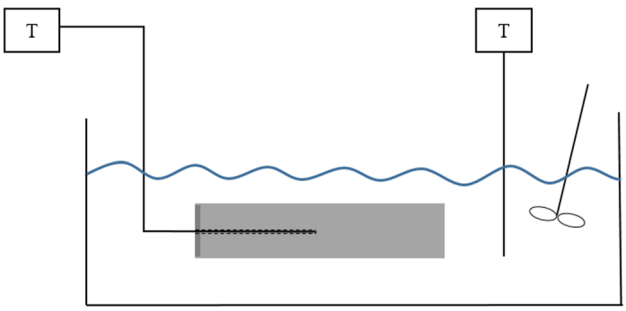

Fig. 4 Diagram of 30 °C water bath showing temperature probes, stirrer and cylinder placement

The temperature change with time for an aluminum cylinder with identical dimensions was also recorded in the same manner. The aluminum has a well characterized and relatively high thermal conductivity of 236 W/(m K), density of 2710 kg/m^3, and specific heat of 902 J/(kg K) at 20 °C. Thus, the aluminum experiment provided a means of obtaining an accurate value for the convective heat transfer coefficient that was not easily obtained for the ABS cylinders due to their low thermal conductivity. The convective heat transfer coefficient obtained in this experiment was therefore used when regressing the effective thermal conductivity of the ABS cylinders.

Due to the high conductivity of aluminum, the data logger was programmed to record a temperature every second. The results were averaged over 4 trials in the hot water bath.

3. Results

The following results were obtained for heating of the catalyst substrates originally at a temperature of 273 ± 0.5 K environment. The cylinders were placed into a hot water bath at 303 ± 0.5 K. The data were averaged over three trials for the experiments with the ABS cylinders. The data were averaged over four trials for the experiments conducted on the aluminum cylinder.

It is clear from Fig. 5 that the solid model had the fastest response. The squares with gap took the longest time to respond, which would be attributed to the fact that it has the least volume of ABS material and the least paths for heat conduction. Heat transfer rates are known to be higher in turbulent flow environments than in stagnant or laminar flow environments as a result of the vigorous mixing of the fluid (Ref 24).

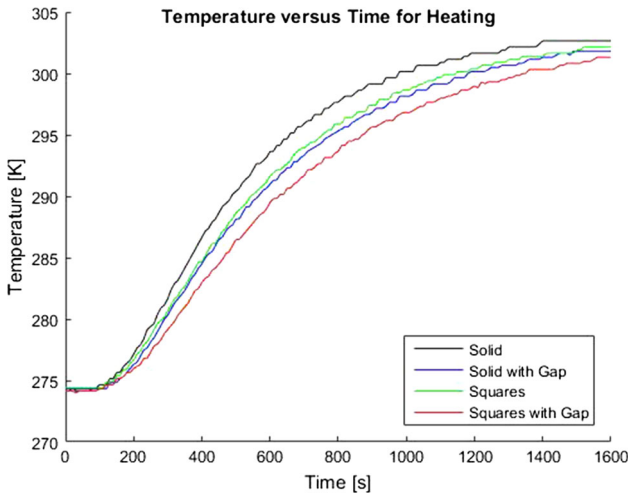

Fig. 5 Heating of ABS catalyst substrates

For heating, the squares (without the gap) had a slightly faster response than the solid with gap. The squares had a faster response than the solid with gap (Fig. 6, 7, 8, 9, 10).

The results for the heating of the aluminum cylinder are given below.

The highly conductive metal cylinder (in Fig. 6) reached a temperature of 303 K in approximately 50 s. Similar to the ABS experiments, this indicated that the conditions within the heated water bath were relatively uniform and can be considered well-mixed.

3.1 Analysis of Results

The results using ABS cylinders clearly demonstrate how dominant conduction is, and that greater wall integration results in greater agreement with the one-dimensional model. Performance of the monolith was superior when conduction pathways were more prevalent, and convective heat transfer was at a relative minimum. The solid monolith gave the best performance, followed by the solid monolith with gap, followed by the squares monolith, followed by the squares monolith with gap.

Table 3 compares parameters important for catalysis and lists the different geometries.

Later, we detail a path forward for more characterization tests with structures that have more favorable properties when it comes to catalysis (i.e., higher surface area to volume ratio, higher void fraction, and a higher thermal conductivity).

As a first approximation, each cylinder can be analyzed using a continuum model which assumes an effective thermal conductivity. In other words, the cylinder is modeled as a solid and only temperature variations in the radial dimension need to be considered as a function of time because of the chosen aspect ratio. The benefit of using this approach is that the transient one-dimensional conduction model has an analytical solution which can be used to iteratively determine the effective

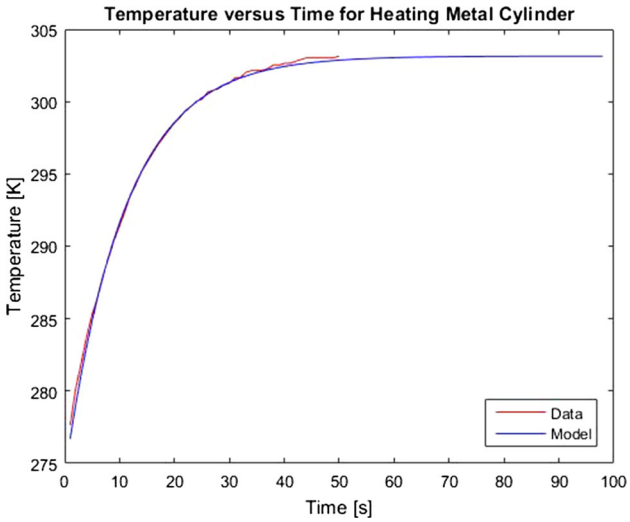

Fig. 6 Experimental results for heating a metal cylinder shown with model results

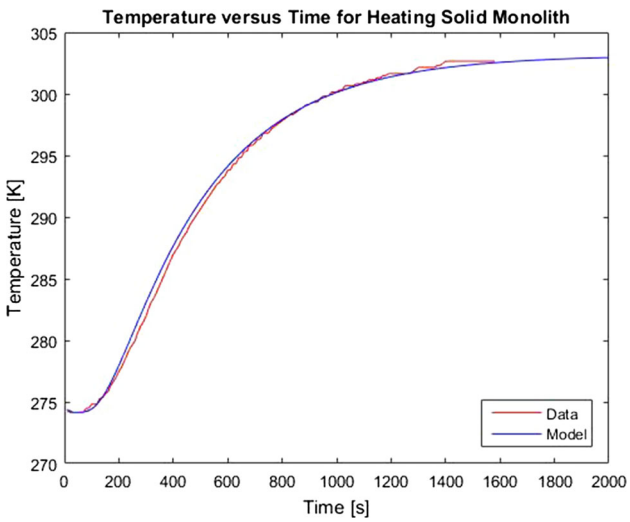

Fig. 7 Temperature vs. time plots shown for the ABS solid monolith and its agreement with a one-dimensional heat conduction model

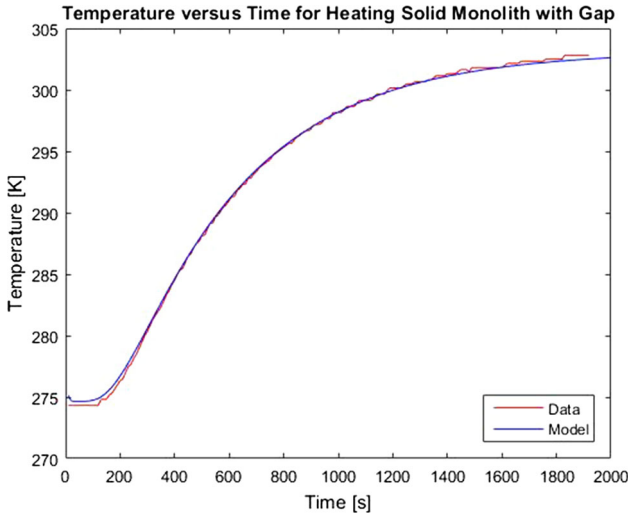

Fig. 8 Temperature vs. time plots shown for the ABS solid monolith with a gap and its agreement with a one-dimensional heat conduction model

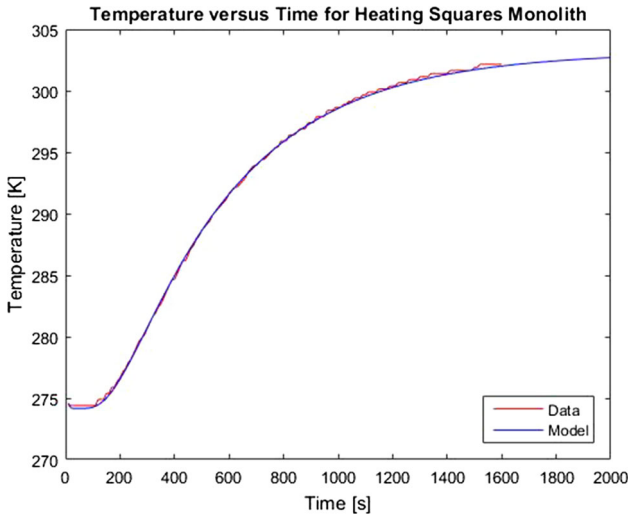

Fig. 9 Temperature vs. time plots shown for the ABS squares monolith and its agreement with a one-dimensional heat conduction model

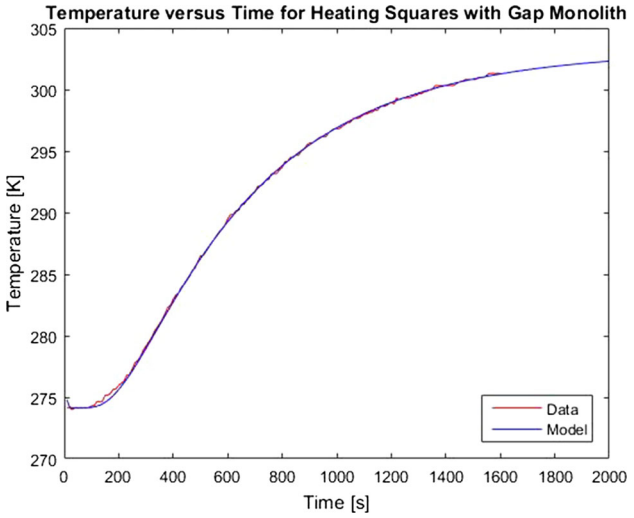

Fig. 10 Temperature vs. time plots shown for the ABS squares monolith with a gap and its agreement with a one-dimensional heat conduction model

thermal conductivity of each cylinder, while accounting for the change in void fraction and bulk density of each cylinder.

3.2 Developing the Model

Equation 1 represents a one-dimensional transient heat conduction in cylindrical coordinates and describes the temperature distribution, $T[t,r]$ as a function of time, t, and radial position, r.

$$\frac{1}{r}\frac{\mathrm{d}}{\mathrm{d}r}\left(r\frac{\mathrm{d}T}{\mathrm{d}r}\right)=\frac{1}{\alpha_{\mathrm{eff}}}\frac{\mathrm{d}T}{\mathrm{d}t} \quad \text{(Eq 1)}$$

For the model development, it is assumed that a long cylinder of radius, $r_0 = 0.0175$ m, initially ($t = 0$) at a uniform temperature of $T_i = 273$ K, is placed horizontally in a medium at a constant temperature $T_\infty = 303$ K and kept in the medium for $t > 0$. Heat transfer occurs between the cylinder and the environment via convection with a uniform and constant heat transfer coefficient, $h\left[\frac{\mathrm{W}}{\mathrm{m^2K}}\right]$. The difference between T_∞ and T_i initiates a temperature gradient and hence in the case of heating induces heat conduction from the walls of the cylinder to the center line. This is dependent on the effective thermal diffusivity $\alpha_{\mathrm{eff}}\left[\frac{\mathrm{m^2}}{\mathrm{s}}\right]$ of the material. The model assumes perfect uniformity of the cylinder structure about the center line at $r = 0$. Hence, the temperature profile is symmetrical about the center (axial) axis.

The following boundary conditions are applied to Eq 1, at the surface, $r = r_0$:

$$k_{\mathrm{eff}}\frac{\mathrm{d}T}{\mathrm{d}r}[t,r_0]=h(T_\infty - T[t,r_0]) \quad \text{(Eq 2)}$$

where $k_{\mathrm{eff}}\left[\frac{\mathrm{W}}{\mathrm{mK}}\right]$ is the effective thermal conductivity. Further, at the center, $r = 0$, the symmetry condition can be described by:

$$\frac{\mathrm{d}T}{\mathrm{d}r}[t,0]=0 \quad \text{(Eq 3)}$$

Via separation of variables, the following analytical solution can be found (Ref 5):

$$\theta[\tau,r]=\sum_{m=1}^{\infty}\frac{2}{\beta_m}\frac{J_1(\beta_m)J_0(\beta_m r/r_0)}{J_0^2(\beta_m)+J_0^2(\beta_m)}e^{-\beta_m^2\tau} \quad \text{(Eq 4)}$$

J_0 and J_1 are Bessel functions, and because the thermocouple is placed at the center of the cylinder, $r = 0$ then $J_0(\beta_m r/r_0) = J_0(0) = 1$ and the analytical solution reduces to:

$$\theta[\tau,0]=\sum_{m=1}^{\infty}\frac{2}{\beta_m}\frac{J_1(\beta_m)}{J_0^2(\beta_m)+J_0^2(\beta_m)}e^{-\beta_m^2\tau} \quad \text{(Eq 5)}$$

The dimensionless time or Fourier number, τ, is given in Eq 6.

$$\tau=\frac{\alpha_{\mathrm{eff}}t}{r_0^2} \quad \text{(Eq 6)}$$

where the effective thermal diffusivity, α_{eff}, can be calculated by Eq 7.

$$\alpha_{\mathrm{eff}}=\frac{k_{\mathrm{eff}}}{(1-\epsilon)\rho C_P} \quad \text{(Eq 7)}$$

where ε is the void fraction, $\rho = 1038\frac{\mathrm{kg}}{\mathrm{m^3}}$ is the density and $C_P = 1470\frac{\mathrm{J}}{\mathrm{kgK}}$ is the specific heat of ABS plastic. Values for β_m are found by determining the roots of Eq 8.

$$\beta_m J_1(\beta_m) - Bi J_0(\beta_m) = 0 \quad \text{(Eq 8)}$$

where Bi is the Biot number as follows:

$$Bi=\frac{hr_0}{k_{\mathrm{eff}}} \quad \text{(Eq 9)}$$

Dimensionless temperature, $\theta[\tau,r]$, is defined in Eq 10.

$$\theta=\frac{T[t,r]-T_\infty}{T_i-T_\infty} \quad \text{(Eq 10)}$$

Via substitution of Eq 10 into Eq 5, the following relationship is achieved.

$$T[t,0]=T_\infty+(T_i-T_\infty)\sum_{m=1}^{\infty}\frac{2}{\beta_m}\frac{J_1(\beta_m)}{J_0^2(\beta_m)+J_0^2(\beta_m)}e^{-\beta_m^2\tau} \quad \text{(Eq 11)}$$

Equation 11, which describes the temperature at the center of the cylinder as a function of time, is used to produce an analytical model that was then regressed to determine the effective thermal conductivity of the cylinder.

3.3 Data Regression to the Model

For each of the ABS cylinders, the model was regressed onto the data, which were recorded every 10 s from 300 to 1500 s, in order to determine the effective thermal conductivity. This was carried out by iteratively varying the effective thermal conductivity until the sum of squares error was minimized. For heating, the value for the convective heat transfer coefficient was set at 2053 W/(m^2 K) as determined by the experiments carried out on a solid aluminum cylinder. For the ABS cylinders, only the thermal conductivity was allowed to vary as this poses the greatest resistance to heat transfer. Because of the low thermal conductivity of this material, the model was not sufficiently sensitive to independently determine the value of h. The results are given in Table 4.

Table 3 ABS properties of tested monoliths

Material	Stratasys ABS*plus*-proprietary plastic				
Description	**Unit**	**Solid**	**Solid with gap**	**Squares**	**Squares with gap**
Outer diameter	mm	35	35	35	35
Height	mm	140	140	140	140
SA/V ratio	mm^{-1}	0.02	0.24	0.34	0.65
Void fraction	…	0	0.12	0.13	0.25
Pore size	mm	N/A	N/A	1.9	1.9

Table 4 Effective thermal conductivity of tested monoliths

Description	Unit	Solid	Solid with gap	Squares	Squares with gap
Effective thermal conductivity	W/(m K)	0.223	0.159	0.164	0.122
Error (L_2-norm)	…	1.31E−04	4.69E−05	4.96E−05	3.93E−05
Error (L_∞-norm)	K	1.1	0.3	0.4	0.3

Table 5 Different types of ABS and their thermal conductivity

Type of ABS	Thermal conductivity, W/(m K)
ABS, heat resistant, molded	0.128-0.200 (Ref 21)
ABS, unreinforced, flame retardant	0.173-0.200 (Ref 23)
ABS, impact grade, molded	0.150-0.200 (Ref 22)
ABS, extruded	0.150-0.200 (Ref 20)
ABS, injection molding grade, heat resistant	0.188-0.334 (Ref 11)

Table 6 Effect of the gap on effective thermal conductivity

Description	Solid with gap: solid, %	Squares with gap: squares, %
Percentage change in conductivity	71	74
Percentage change in bulk density	88	86

It is clear from Table 4 that the model was successfully regressed onto the data for all cases. The average L_2- norm error for regression of the heating experiment was 6.67×10^{-5}, and the maximum absolute difference (L_∞-norm) between the regressed model and the experimental data varied from 0.3 to 1.1 K. From analysis of Table 4, the *solid* cylinder is shown to have the highest thermal conductivity of 0.223 W/(m K). The lowest thermal conductivity is the *squares with gap* which has a value of 0.122 W/(m K). Both of these results follow the expected trend.

Since these experiments were conducted with ABS that has been 3D-printed using FDM, it is useful, as a comparison, to include some values for solid thermal conductivity of injection-molded ABS. Typical values of thermal conductivity vary widely for ABS and are between 0.187 and 0.332 W/(m K) (Ref 8). Specific types of ABS and their thermal conductivities are listed in Table 5. The 3D-printed *solid* monolith shows good agreement with these ranges. As FDM 3D-printed parts have mechanically anisotropic properties due to the layer-wise method of manufacture, it is assumed that there is some variation in thermal conductivity along the length of the printed monolithic structures (Ref 36). The plastic thermal conductivity will also vary with temperature; experiments were thus carried out as a function of cooling or heating over a range of temperatures, between 0 and 30 °C.

The *squares* cylinder is shown to have a greater thermal conductivity than the *solid with gap*. These values are 0.164 and 0.159 W/(m K), respectively. The *squares* provide direct paths for conductive heat transfer from the tube inner wall, while the *solid with gap* relies on convective heat transfer alone over the air gap or clearance. As air has a lower thermal conductivity than the plastic, the gap acts as the primary limiting mechanism to heat transfer.

Comparing the conductivities of the *solid* to the *solid with gap* and the conductivities of the *squares* to the *squares with gap* indicates the effect of bridging the clearance between the catalyst support and inner tube wall. This clearance is designed to be identical in both cases. Table 6 shows that for the solid cylinders, the existence of the gap reduces the effective thermal conductivity to 71% of the ideal case. For the squares concepts, this value is 74%, and this change in conductivity cannot be explained by the reduction in bulk density (i.e., increase in void space) alone. As the gap to no-gap change in conductivity results are similar for the two comparisons, it illustrates that the experimental procedures were consistent over the trials. It also reveals that the AM successfully replicated the gap which had been designed in SolidWorks as previously described.

Tronconi et al. (Ref 35) found that a significant increase in the inside wall heat transfer coefficient was possible with suitable packaging methods aimed at reducing the clearance between the monolith and reactor tube. With no special packing, a heat transfer coefficient of 220 W/(m^2 K) resulted for a highly conductive copper monolith, while careful manipulation of the packing produced values of 400-500 W/(m^2 K).

The results show that the ABS monolith effective thermal conductivity increased by 34-40% with complete elimination of the gap. However, unlike work carried on highly conductive material, the thermal conductivity of ABS is still such that this

represents a major resistance to heat transfer. To a first approximation, the inside wall heat transfer coefficient for the ABS cylinders can be estimated by dividing the effective thermal conductivity by the gap width, and this results in values of 64 and 83 W/(m^2 K) for the squares with gap and solid with gap samples, respectively. This is substantially smaller than the outside wall heat transfer coefficient of 2053 W/(m^2 K), and if the cylinders are printed in a highly conductive material (Ref 35), it is likely that inside wall heat transfer coefficients even greater than 500 W/(m^2 K) can be achieved once the gap is mitigated.

4. Conclusions

This paper focused on thermally characterizing the cylinders printed in ABS*plus* and the effect of having a gap between the monolithic structure and the pseudo-wall of the structure and printing a continuous structure as illustrated in Fig. 3. The presence of the gap introduces a drop in the overall effective thermal conductivity of the structure relative to the solid structure. The presence of greater internal surface area in the form of square features also decreases the thermal conductivity of the monoliths. The monolith with the squares and a gap has a lower thermal conductivity than the monolith with the squares and no gap. This is attributed to the increased resistance to heat transfer via convection across the air gap over conduction. The air inside of the sealed monoliths has a much lower thermal conductivity than the ABS plastic by about an order of magnitude at the conditions of relevance (Ref 24).

Using a transient one-dimensional conduction model, which assumes each cylinder consisted of a single material with an effective thermal diffusivity generated excellent agreement between the regressed model and the experimental results, is a useful way of determining each cylinders' effective thermal conductivity. Overall, it was found that for a square-hole monolith, the effective thermal conductivity could be increased from 0.122 to 0.164 W/(m K) by incorporating the reactor wall into the monolith through the use of additive manufacturing (AM). AM provided the ability to eliminate the clearance requirement at the interface of the hypothetical monolith and reformer tube. Overall, this equated to a 34% increase in the effective thermal conductivity of the monolithic ABS structure. A similar improvement of 40% was found for the solid base case cylinders, where the solid ABS cylinder which represented a perfect heat conduction scenario yielded a thermal conductivity of 0.223 W/(m K). In contrast, the solid cylinder with the gap clearance had a smaller effective thermal conductivity of 0.159 W/(m K).

Future work will include the testing of multiple geometries printed in metal to use a material that has a higher thermal conductivity. These geometries will have higher void fractions, which should represent a decrease in pressure drop relative to the previously tested structures and much higher surface area to volume ratios which are desirable in catalytic applications. In addition, work is underway to build a printer utilizing 3DP technology to expand the material choices for these geometries, with the capability of multi-material additive manufacturing. With multi-material additive manufacturing, it will be possible to integrate the metal reactor wall with the ceramic catalyst substrate to improve thermal performance of the reaction and to reduce the typically extreme temperature gradients present in steam–methane reforming. It should also be possible to use multi-material printing to fully integrate the catalyst into the substrate as part of the printing process itself.

Appendix: The Effect of the Polypropylene Film

In order to determine the effect of the polypropylene film on the overall effective thermal conductivity, the cylinder was treated as a composite plane wall with heat transfer at the surfaces. The heat transfer area A(m^2) is assumed to be the surface area of the cylinder, neglecting the ends. The correlation was performed for the solid cylinder, where the thermal conductivity k_1 of the ABS was found to be 0.22 W/(m K). The thermal conductivity k_2 of polypropylene is 0.16 W/(m K).

The following equation is employed to account for both ABS and polypropylene (Ref 37).

$$C = \frac{A}{\frac{1}{h_A} + \frac{d_1}{k_1} + \frac{d_2}{k_2}} \quad \text{(Eq 12)}$$

where C is the thermal conductance in W/K and d_1 and d_2 are the "thicknesses" of the ABS plastic and polypropylene, respectively. This is then compared to Eq 13 which accounts for the ABS material only.

$$C = \frac{A}{\frac{1}{h_A} + \frac{d_1}{k_1}} \quad \text{(Eq 13)}$$

The conductance for the ABS was found to be 0.1951 W/K while the conductance for the composite substrate was very slightly reduced at 0.1947 W/K. Therefore, the thermal conductance of the composite is 99.78% that of the singular ABS material, showing a negligible effect. This assumption is therefore considered valid.

References

1. 3D Printing: The New Design of Safety. *NBBI Bull. Tech. J. Natl. Board Boiler Press. Vessel Insp.*, 2013, **68**, p 24–31
2. M. Balat, Potential Importance of Hydrogen as a Future Solution to Environmental and Transportation Problems, *Int. J. Hydrog. Energy*, 2008, **33**(15), p 4013–4029. doi:10.1016/j.ijhydene.2008.05.047
3. S.A. Bhat and J. Sadhukhan, Process Intensification Aspects for Steam Methane Reforming: An Overview, *AIChE J.*, 2009, **55**(2), p 408–422. doi:10.1002/aic.11687
4. T. Boger and A. Heibel, Heat Transfer in Conductive Monolith Structures, *Chem. Eng. Sci.*, 2005, **60**(7), p 1823–1835. doi:10.1016/j.ces.2004.11.031
5. Y.A. Çengel and A.J. Ghajar, *Heat and Mass Transfer: Fundamentals & Applications*, McGraw-Hill Education, New York, 2015
6. B.J. de Gans, P.C. Duineveld, and U.S. Schubert, Inkjet Printing of Polymers: State of the Art and Future Developments, *Adv. Mater.*, 2004, **16**(3), p 203–213. doi:10.1002/adma.200300385

7. Z.C. Eckel, C. Zhou, J.H. Martin, A.J. Jacobsen, W.B. Carter, and T.A. Schaedler, Additive Manufacturing of Polymer-Derived Ceramics, *Science*, 2016, **351**(6268), p 58–62. doi:10.1126/science.aad2688
8. *Engineering Thermoplastics: Properties and Applications, Plastics Engineering (Book 8)*, Vol. 8, edited by J.M. Margolis (D.E. Hudgin, Series Ed.) (CRC Press, New York, 1985), 408 pp
9. R.J. Farrauto, Y. Liu, W. Ruettinger, O. Ilinich, L. Shore, and T. Giroux, Precious Metal Catalysts Supported on Ceramic and Metal Monolithic Structures for the Hydrogen Economy, *Catal. Rev. Sci. Eng.*, 2007, **49**(2), p 141–196. doi:10.1080/01614940701220496
10. C. Fee, S. Nawada, and S. Dimartino, 3D Printed Porous Media Columns with Fine Control of Column Packing Morphology, *J. Chromatogr. A*, 2014, **1333**, 18–24. doi:10.1016/j.chroma.2014.01.043
11. E. Fundamentals, *ABS Material Properties* (2014). http://www.efunda.com/materials/polymers/properties/polymer_datasheet.cfm?MajorID=ABS&MinorID=7
12. G. Groppi and E. Tronconi, Honeycomb Supports with High Thermal Conductivity for Gas/Solid Chemical Processes, *Catal. Today*, 2005, **105**(3–4), p 297–394. doi:10.1016/j.cattod.2005.06.041
13. N. Hopkinson and P. Dickens, Emerging Rapid Manufacturing Processes, in *Rapid Manufacturing* (Wiley, 2006), p. 55-80
14. J.B. Kaczynski, *Three Dimensional Printing* (2000). http://www.mit.edu/~tdp/whatis3dp.html
15. R. Klein, *Laser Welding of Plastics*, Wiley-VCH Verlag & Co, Weinheim, Germany, 2012
16. A. Kosmač, *Stainless Steels at High Temperatures* (2012). http://www.bssa.org.uk/cms/File/StainlessSteels_at_HighTemperatures_EN.pdf
17. V.A. Kozlov, V.V. Toporova, I.A. Kosnareva, and E.A. Zinigrad, Variation of the Thermal Conductivity of Copper Powder During Drying, *Sov. Powder Metall. Met. Ceram.*, 1973, **12**(1), p 9–12. doi:10.1007/BF00803967
18. J.P. Kruth, P. Mercelis, J. Van Vaerenbergh, L. Froyen, and M. Rombouts, Binding Mechanisms in Selective Laser Sintering and Selective Laser Melting, *Rapid Prototyp. J.*, 2005, **11**(1), p 26–36
19. J.A. Lewis, J.E. Smay, J. Stuecker, and J. Cesarano, III, Direct Ink Writing of Three-Dimensional Ceramic Structures, *J. Am. Ceram. Soc.*, 2006, **89**(12), p 3599–3609. doi:10.1111/j.1551-2916.2006.01382.x
20. L. MatWeb, *Overview of Materials for Acrylonitrile Butadiene Styrene (ABS), Extruded* (2017a). http://www.matweb.com/search/DataSheet.aspx?MatGUID=3a8afcddac864d4b8f58d40570d2e5aa&ckck=1
21. L. MatWeb, *Overview of Materials for Acrylonitrile Butadiene Styrene (ABS), Heat Resistant, Moulded* (2017b). http://www.matweb.com/search/DataSheet.aspx?MatGUID=2d146961e7274da686aafd5470e03dee&ckck=1
22. L. MatWeb, *Overview of Materials for Acrylonitrile Butadiene Styrene (ABS), Impact Grade, Molded* (2017c). http://www.matweb.com/search/DataSheet.aspx?MatGUID=0177ea648dd340abb81c25b4efe613ad
23. L. MatWeb *Overview of Materials for Acrylonitrile Butadiene Styrene (ABS), Unreinforced, Flame Retardant* (2017d). http://www.matweb.com/search/datasheet.aspx?MatGUID=53d216d78a2c46e08bbe1ccf54252f3e&ckck=1
24. A.F. Mills, *Basic Heat and Mass Transfer*, Vol 2nd, Prentice Hall, Upper Saddle River, 1999
25. J.S.S. Mohammadzadeh and A. Zamaniyan, Catalyst Shape as a Design Parameter—Optimum Shape for Methane-Steam Reforming Catalyst, *Chem. Eng. Res. Des.*, 2002, **80**(4), p 383–391. doi:10.1205/026387602317446425
26. S. Nawada, C. Fee, and S. Dimartino, *The Effects of Bead Overlap on Chromatographic Performance in 3d Printer Packed Bed Columns*, International Labmate, 2014, p 18–20. Retrieved from https://www.labmate-online.com/article/chromatography/1/suhas_nawada_simone_dimartino_conan_fee/the_effects_of_bead_overlap_on_performance_of_3d_printed_packed_bed_columns/1609
27. J.R. Rostrup-Nielsen, Catalytic Steam Reforming, *Catalysis: Science and Technology*, J.R. Anderson and M. Boudart, Eds., Springer, Berlin, Heidelberg, 1984, p 1–117
28. J.R. Rostrup-Nielsen, L.J. Christiansen, and J.-H. Bak Hansen, Activity of Steam Reforming Catalysts: Role and Assessment, *Appl. Catal.*, 1988, **43**(2), p 287–303
29. J.R. Rostrup-Nielsen and T. Rostrup-Nielsen, Large-Scale Hydrogen Production, *CATTECH*, 2002, **6**(4), p 150–159. doi:10.1023/A:1020163012266
30. J.R. Rostrup-Nielsen, J. Sehested, and J.K. Nørskov, Hydrogen and Synthesis Gas by Steam- and CO_2 Reforming, *Adv. Catal.*, 2002, **47**, p 65–139
31. E. Sachs, M. Cima, J. Cornie, D. Brancazio, J. Bredt, A. Curodeau, and S. Michaels, Three-Dimensional Printing: The Physics and Implications of Additive Manufacturing, *CIRP Ann. Manuf. Technol.*, 1993, **42**(1), p 257–260. doi:10.1016/S0007-8506(07)62438-X
32. M. Schwentenwein and J. Homa, Additive Manufacturing of Dense Alumina Ceramics, *Int. J. Appl. Ceram. Technol.*, 2014, **12**(1), p 1–7. doi:10.1111/ijac.12319
33. M. Sheng, H. Yang, D.R. Cahela, and B.J. Tatarchuk, Novel Catalyst Structures with Enhanced Heat Transfer Characteristics, *J. Catal.*, 2011, **281**(2), p 254–262. doi:10.1016/j.jcat.2011.05.006
34. P. Sitthi-Amorn, J.E. Ramos, Y. Wang, J. Kwan, J. Lan, W. Wang and W. Matusik, in *MultiFab: A Machine Vision Assisted Platform for Multi-material 3D printing*. Paper presented at the SIGGRAPH 2015, Los Angeles Convention Center (2015)
35. E. Tronconi, G. Groppi, T. Boger, and A. Heibel, Monolithic Catalysts with 'High Conductivity' Honeycomb Supports for Gas/Solid Exothermic Reactions: Characterization of the Heat-Transfer Properties, *Chem. Eng. Sci.*, 2004, **59**, p 4941–4949. doi:10.1016/j.ces.2004.07.018
36. M.S. Uddin, M.F.R. Sidek, M.A. Faizal, R. Ghomashchi, and A. Pramanik, Evaluating Mechanical Properties and Failure Mechanisms of Fused Deposition Modeling Acrylonitrile Butadiene Styrene Parts, *J. Manuf. Sci. Eng.*, 2017, **139**(8), p 081018. doi:10.1115/1.4036713
37. H.Y. Wong, *Handbook of Essential Formulae and Data on Heat Transfer for Engineers*, Longman, London, 1977
38. A. Zaleski, *GE's Bestselling Jet Engine Makes 3-D Printing a Core Component* (2015). http://fortune.com/2015/03/05/ge-engine-3d-printing/
39. A. Zamaniyan, Y. Mortazavi, A.A. Khodadadi, and H. Manafi, Tube Fitted Bulk Monolithic Catalyst as Novel Structured Reactor for Gas–Solid Reactions, *Appl. Catal. Gen.*, 2010, **385**(1–2), p 214–223. doi:10.1016/j.apcata.2010.07.014